Lasers in Manufacturing Conference 2023

High nitrogen steels produced by PBF-LB/M –
Influence of particle size distribution and process parameters on melting behavior of additivated steel powders

Felix Radtke[a,*], Louis Becker[b], Simone Herzog[a], Jonathan Lentz[b], Sebastian Weber[b], Christoph Broeckmann[a]

[a] Institute of Applied Powder Metallurgy and Ceramics (IAPK); Augustinerbach 4, 52062 Aachen, Germany
[b] Chair of Materials Technology (LWT); Universitätsstraße 150, 44801 Bochum, Germany

Abstract

Additivated powders allow an extension of suitable materials for the powder bed fusion laser beam process (PBF-LB/M). High nitrogen steel (HNS) powders and components are limited by the nitrogen solubility of the melt and thus possible interstitial solid solution strengthening. In this study, Si_3N_4 powder is added to the austenitic steel powder AISI 304L. The PBF-LB/M process is adapted to shape components in which the Si_3N_4 particles are only partially dissolved in the melt. In a subsequent hot isostatic pressing (HIP) process, nitrogen diffuses into the component, taking advantage of the high nitrogen solubility of the austenite. The particle size distribution of the powders and the process parameters of the PBF-LB/M process were varied in the context of this work. Undissolved Si_3N_4 particles are identified and the total nitrogen contents are quantified to evaluate the process parameters and melting behavior of Si_3N_4 additivated austenitic steel powders. The final material is evaluated regarding density and microstructure.

Keywords: PBF-LB/M; high nitrogen steels; 304L Si_3N_4; additivation; melting behavior

1. Introduction

Additivation of commercially available powders for laser-based additive manufacturing with PBF-LB/M has gained increasing interest in the research community. The main objective is to overcome the limited range of

---

* Corresponding author.

available steel grades for PBF-LB/M, such as AISI 316L [1], 17-4PH [2] or 18-Ni300 [3]. In-situ alloying in the. PBF-LB/M process meets these requirements while eliminating the need for expensive special atomization The PBF-LB/M processing of steels with additives has already been the subject of several studies. These have in common the intention to improve the base materials, but currently there is still a lack of used powders and target alloy systems. Furthermore, the homogeneity of the samples represents a research point, including pre-processes, in-processes and post-processes to avoid demixing effects [4–7]. The objective of this work is to produce high nitrogen steels (HNS) by adding silicon nitride (Si_3N_4) to austenitic stainless steel (ASS) powders in the PBF-LB/M process. Figure 1 illustrates the required process steps with particular emphasis on the PBF-LB/M process, which is the focus of this paper.
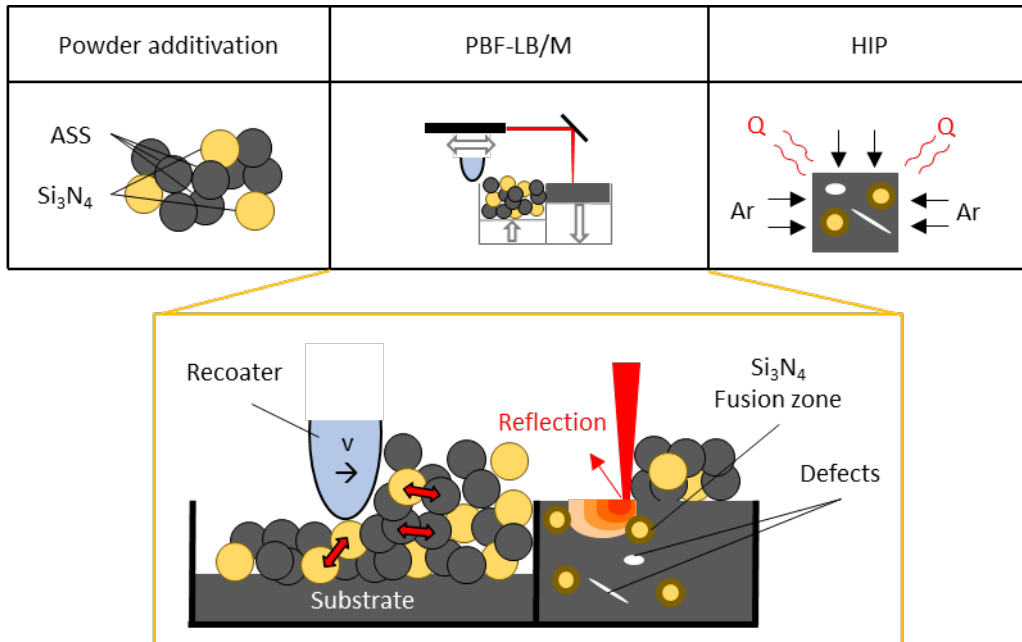

Fig. 1. Process chain for the development of HNS using additivated ASS powder, PBF-LB/M process and HIP post densification

2. Material and Methods

2.1. Powder materials

X2CrNi18-9 (1.4307, AISI 304L) gas atomized austenitic stainless steel (ASS) powder delivered by Carpenter Additive was used as the matrix material in this word. The powder was sieved to the fraction of 20 – 63 µm and dried at 105 °C for 30 minutes under air atmosphere. The ASS was additivated with 0.9 wt.-% Si_3N_4 powder (FuseNano) of a particle size between 36 and 71 µm. The additivated powder is hereafter referred to ASS+. The chemical compositions (extracted from the datasheets/calculated), flow rates (FR_H) according to ASTM B213, and apparent densities (AD) according to ASTM B212 are given in Table 1.

Table 1. Chemical composition and powder properties of X2CrNi18-9 (Carpenter Additive), Si_3N_4 (FuseNano) and ASS+ (additivated X2CrNi18-9)

	Chemical composition [wt.-%]									FR_H [s/50g]	AD [g/cm³]
	C	Si	Mn	Cr	Ni	Mo	O	N	Fe		
ASS	0.028	0.66	1.2	18.4	9.2	0.01	0.03	0.08	Bal.	19	4.25
Si_3N_4	-	Bal.	-	-	-	-	0.7	33	-	-	-
ASS+	0.028	1.25	1.2	18.2	9.1	0.01	0.05	0.45	Bal.	18	3.91

2.2. PBF-LB/M processing

A SLM 100 (Realizer GmbH) was used to produce cuboids (10x10x10 mm³). The emitted radiation has a wavelength of 1070 ± 2.5 nm and reaches a maximum laser power of 200 W. The layer thickness d_l was 50 µm, the preheating temperature was set to 200 °C, and the hatch distance d_H was 0.1 mm. All experiments were performed under nitrogen atmosphere. The process parameters exposure time t_e, point distance d_p, and laser power P_L were varied and are represented in the volume energy density E_v calculated by equations (1) and (2).

$$v_s = \frac{d_p}{t_e} \tag{1}$$

$$E_v = \frac{P_L}{v_s \cdot d_H \cdot d_l} \tag{2}$$

2.3. Analysis of powder materials

The particle size distribution (PSD) of the used powder materials was measured by a laser scattering PSD analyzer LA-950 (Horiba Ltd.) under dry conditions. Its relative humidity was determined with a moisture analyzer DBS (Kern & Sohn GmbH). The analysis of the N content is used as an indicator for the amount of Si_3N_4 particles in the additivated powders and PBF-LB/M processed specimens. It was measured by carrier gas hot extraction on an ONH analyzer (ELTRA GmbH).

2.4. Microscopy

Light optical microscopy was performed on an Axio Imager M2m microscope (Carl Zeiss Microscopy Deutschland GmbH). ImageJ software (version 1.53) was used to analyse the relative density, pore structure, and circularity of the pores. Etched (V2A, 70 °C, 50 s) specimens were used for microstructure characterization and grain analysis. A scanning electron microscope of type JSM-6400 (JEOL Ltd.) was used to qualitatively describe the powder morphology and additivated powder homogeneity. Electron backscatter diffraction (EBSD) scans were recorded with a Helios Nano Lab Dual Beam, (Thermo Fisher Scientific). The analysis of EBSD was carried out using TSL OIM Data Collection 7 and OIM Analysis 7 (EDAX, AMETEK). For the evaluation, the phases austenite (a = 3.65 Å) and ferrite (a = 2.87 Å) were considered and illustrated in EBSD maps.

3.   Results and Discussion

3.1. Powder properties

A comparison of pure ASS and ASS+ is shown in Figure 2. The differences are evident in the SEM images, PSD measurements, and the relative humidity.
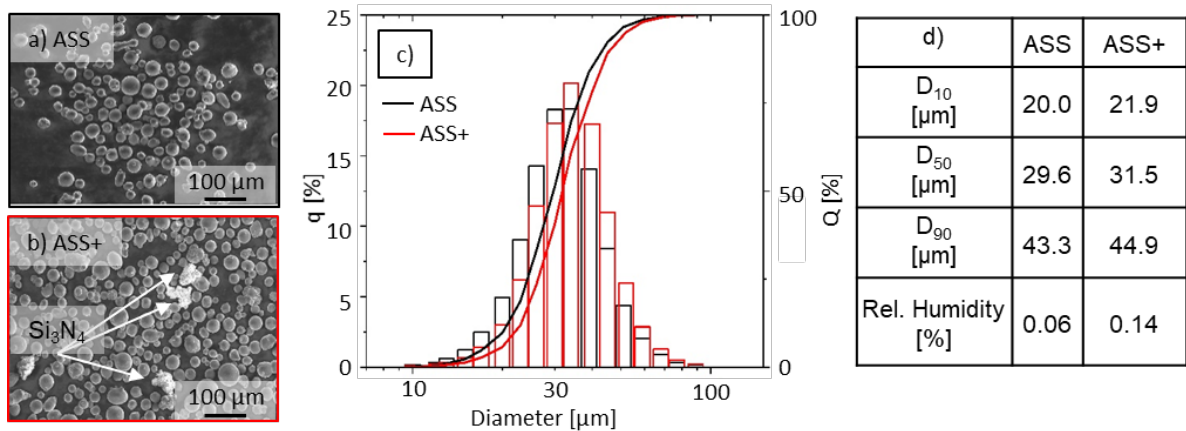

d)	ASS	ASS+
D_{10} [µm]	20.0	21.9
D_{50} [µm]	29.6	31.5
D_{90} [µm]	43.3	44.9
Rel. Humidity [%]	0.06	0.14

Fig. 2. Comparison of ASS and ASS+ powder properties including a) and b) SEM images, c) PSD measurements and d) a table of D10, D50, D90 and relative humidity

Si_3N_4 powder particles can be seen as white flakes in Figure 2 b). They are not cracked, agglomerated or otherwise degenerated. For the ASS+ powder, a homogeneous distribution is observed with a shift of the PSD towards higher particle sizes compared to the ASS powder. The values of D_{10}, D_{50} and D_{90} are slightly higher for the ASS+ powder. In addition, ASS+ powder shows an increasing value of the measured relative humidity compared to ASS. The additivation of hydrophobic Si_3N_4 [8] leads to an increase of the relative humidity. It is not yet clear how the humidity gets into the Si_3N_4 and whether the humidity can be reduced by drying at higher temperatures.

3.2. PBF-LB/M Processing

ASS

In a first step non-additivated X2CrNi18-9 was processed to establish a reference state and to refine a range of optimal process parameters. In Figure 3 a), the relative density of the samples and a mean circularity of the pores are plotted against the volume energy density E_v. An E_v less than 37 J/mm³ leads to the lowest relative density values and the lowest circularity. The energy input is too low to create a stable melt pool, resulting in insufficient connections between the hatches and a high number of lack of fusion defects. Between 37 J/mm³ and < 50 J/mm³ a stable processing window exists resulting in relative densities above 99% and a circularity of the pores around 0.9. The type of defects can be distinguished as lack of fusion defects and gas pores (Figure 3 b). At E_v above 53 J/mm³, gas porosity dominates, which can be identified by the highest value

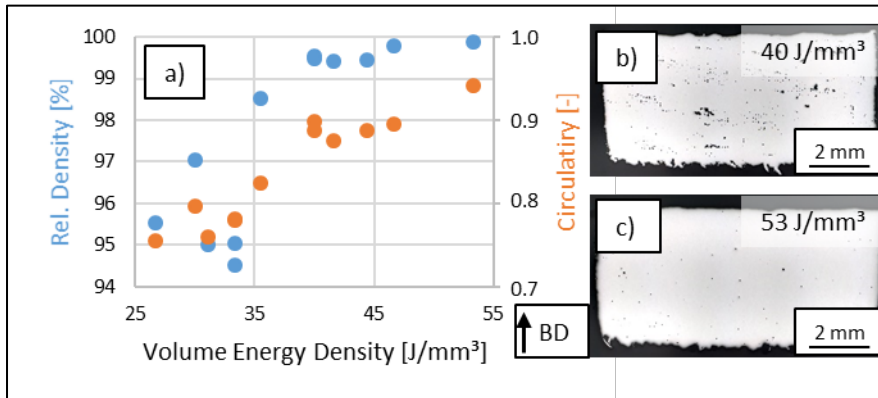of circularity and the light optical microscopic image (Figure 3 c).

Fig. 3. a) Relative density and pore circularity of PBF-LB/M processed ASS powder; light microscope images of specimens produces at a volume energy density of b) 40 J/mm³ and c) 53 J/mm³

ASS+

According to the results of non-additivated ASS, the ASS+ powder is produced at E_v values between 30 J/mm³ and 57 J/mm³. For low volume energy densities below 35 J/mm³, there is a noticeable decrease in relative density. It drops to values below 95 % where closed porosity cannot be guaranteed and HIP post densification is not reasonable. The light optical microscopy images in Figure 4 b) and c) show two specimens produced with the same energy density of 42 J/mm³, but in different building jobs. The results show two different pore structures and analysis values. The relative density varies from 96.2 % to 99.6 % and the value of circularity value varies from 0.81 to 0.88. The light optical microscopy images show a systematic defect band along the building direction (Figure 4 b)) caused by an overlapping scanning strategy, an inhomogeneous distribution of lack of fusion defects in the lower part, and gas pore defects in the upper part of the specimen (Figure 4 c)). This irregular result proves an unstable process and is determined by influencing variables and disturbances that have not yet been understood. The highest level of energy densities higher than 50 J/mm³ shows irregular results for the relative densities and circularity, supporting the assumption of an unstable process.
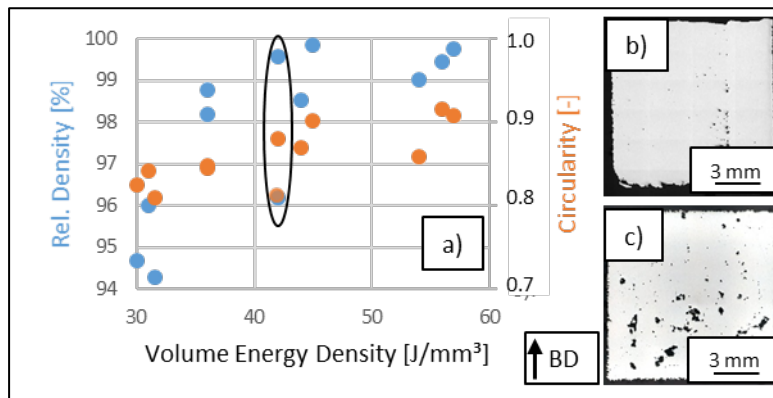

Fig. 4. a) Relative density and pore circularity of PBF-LB/M processed ASS+ powder; b) and c) light microscope images of specimens produces at a volume energy density of 42 J/mm³

3.3. Microstructure analysis

A comparison of the microstructure including EBSD maps and etched specimen images for ASS and ASS+ specimens are shown in Figure 5.
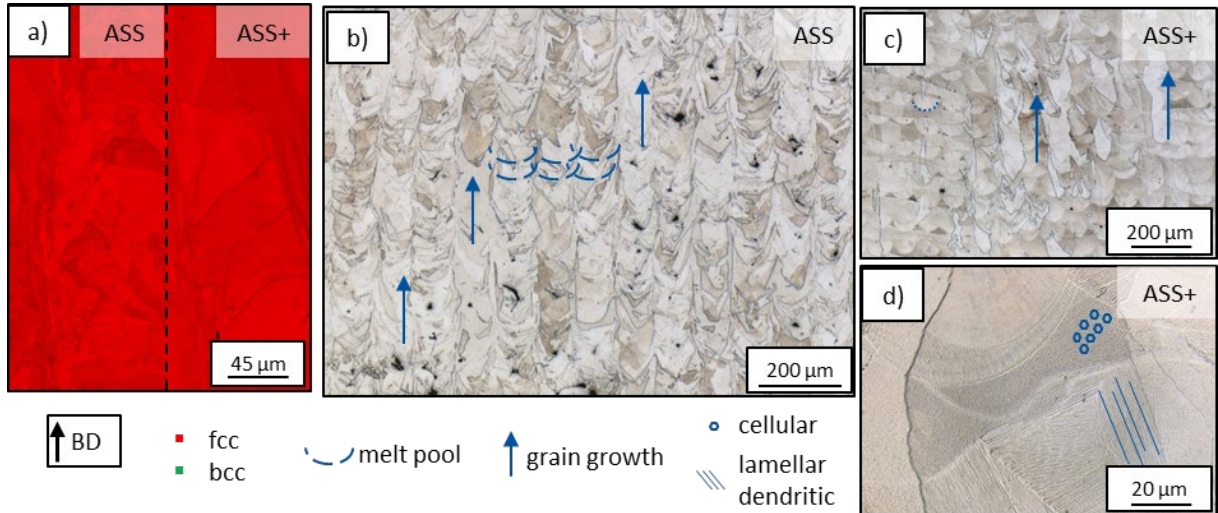

Fig. 5. a) EBSD mappings for ASS and ASS+ specimen; b) etched ASS specimen; c) etched ASS+ specimen; d) etched ASS+ specimen

The EBSD maps in Figure 5 a) show a 100% face centered cubic (fcc) crystal structure for both specimens. The images in b) and c) reveal an austenitic etched microstructure for ASS and ASS+. In addition, the melt pool structure and growth strategy can be seen for the etched specimens. Both samples show grain growth parallel to the building direction (BD) and beyond the melt pools. The melt pools are represented by a semi-circular structure. At a magnification of 1000, microstructure morphologies consisting of columnar dendritic and cellular portions are present (Figure 5 d)). The columnar dendritic grains grow from their nucleation sites at the edges to the center of the melt pools. Microstructure analysis shows no difference between ASS and ASS+ specimens and typical austenitic structures.

3.4. Nitrogen Analysis

To quantify the amount of Si_3N_4 particles within the ASS matrix, the amount of nitrogen of all specimens is measured. Table 2 shows the N contents for the ASS and ASS+ powders and specimens (E_v = 42 J/mm³) in wt.%.

Table 2. N-content of ASS and ASS+ powder and specimens

	ASS Powder	ASS Specimen	ASS+ Powder	ASS+ Specimen
N-Content [wt.-%]	0.084 ± 0.008	0.078 ± 0.011	0.446 ± 0.020	0.085 ± 0.007

The additivation results in an increase of 0.362 wt.-% of nitrogen in the powder material. During processing, a loss of nitrogen of about 0.006 wt.-% for the ASS specimens and about 0.361 wt.-% for the ASS+ specimens is observed. The loss of nitrogen within the ASS+ specimens is exactly the same value as its Si_3N_4

addition. This result shows a complete dissolution of Si_3N_4 particles and outgassing of nitrogen. After the PBF-LB/M process, there are no residual N-donator particles left in the material.

4. Conclusion

The austenitic stainless steel powder X2CrNi18-9 (ASS) was additivated with Si_3N_4 and processed via PBF-LB/M to prepare specimens containing Si_3N_4 particles as N-donator being suitable for a HIP post densification.

- The additivated powder shows higher relative humidity and a shift to larger particles in the particle size distribution
- The processing window for ASS powder lies between 37 J/mm³ and 50 J/mm³
- Additivation with Si_3N_4 reduces the processability significantly within the same processing parameter range
- ASS+ specimens show a high variety in pore structure and an inhomogeneous distribution of pores
- ASS and ASS+ specimens show a typical austenitic grain structure and epitaxial grain growth over several melt pools along the building direction
- The intended increase of the nitrogen content by introducing Si_3N_4 particles could not be proven
- The additional nitrogen content in the Si_3N_4 additivated powder corresponded to the nitrogen loss trough the PBF-LB/M process

The additivation of Si_3N_4 leads to worse powder properties, which results in a reduction of processability by PBF-LB/M. The production of dense, defect free specimens competes with the increase in nitrogen content due to undissolved Si_3N_4 particles. Further research with a shell-core approach will be performed to avoid the N-loss in the specimens when the powder is exposed to the laser beam. The goal of this strategy is the production of dense hulls, therefore HIP-compliant specimens with an increase in nitrogen in the core.

References

[1] Vukkum, V. B.; Gupta, R. K.: Review on corrosion performance of laser powder-bed fusion printed 316L stainless steel: Effect of processing parameters, manufacturing defects, post-processing, feedstock, and microstructure. In: Materials & Design 221 (2022), S. 110874.

[2] Stoudt, M. R.; Campbell, C. E.; Ricker, R. E.: Examining the Relationship Between Post-Build Microstructure and the Corrosion Resistance of Additively Manufactured 17-4PH Stainless Steel. In: Materialia 22 (2022), S. 101435.

[3] Platl, J.; Bodner, S.; Hofer, C.; Landefeld, A.; Leitner, H.; Turk, C.; Nielsen, M.-A.; Demir, A. G.; Previtali, B.; Keckes, J.; Schnitzer, R.: Cracking mechanism in a laser powder bed fused cold-work tool steel: The role of residual stresses, microstructure and local elemental concentrations. In: Acta Materialia 225

(2022), S. 117570.

[4]   Narasimharaju, S. R.; Zeng, W.; See, T. L.; Zhu, Z.; Scott, P.; Jiang, X.; Lou, S.: A comprehensive review on laser powder bed fusion of steels: Processing, microstructure, defects and control methods, mechanical properties, current challenges and future trends. In: Journal of Manufacturing Processes 75 (2022), S. 375–414.

[5]   Mosallanejad, M. H.; Niroumand, B.; Aversa, A.; Saboori, A.: In-situ alloying in laser-based additive manufacturing processes: A critical review. In: Journal of Alloys and Compounds 872 (2021), S. 159567.

[6]   Shoji Aota, L.; Bajaj, P.; Zschommler Sandim, H. R.; Aimé Jägle, E.: Laser Powder-Bed Fusion as an Alloy Development Tool: Parameter Selection for In-Situ Alloying Using Elemental Powders. In: Materials (Basel, Switzerland) 13 (2020) 18.

[7]   Becker, L.; Lentz, J.; Benito, S.; Cui, C.; Ellendt, N.; Fechte-Heinen, R.; Weber, S.: A comparative study of in-situ alloying in laser powder bed fusion for the stainless steel X2CrNiMoN20-10-3. In: Journal of Materials Processing Technology 318 (2023), S. 118038.

[8]   Usenko, A.; Senawiratne, J.: Silicon Nitride Surface Conversion into Oxide to Enable Hydrophilic Bonding. In: ECS Transactions 33 (2010) 4, S. 475–83.